SOCIETY OF PETROLEUM ENGINEERS OF AIME
6200 North Central Expressway
Dallas, Texas 75206

PAPER
NUMBER SPE 3600

THIS IS A PREPRINT --- SUBJECT TO CORRECTION

A Three-Phase, Experimental and Numerical Simulation Study of the Steam Flood Process

By

A. Abdalla and K. H. Coats, Members AIME, INTERCOMP

ABSTRACT

A numerical model of steam-drive oil recovery was developed and tested. The implicit pressure-explicit saturation (IMPES) technique was used to solve the three-phase fluid flow equations for compressible fluids. A method was developed and applied to determine the temperature and the rate of steam condensation implicitly from the heat-balance equation. Both techniques were used in computer simulators for linear and two-dimensional systems.

A steam-injection experimental study was performed in a linear model. The results of this experimental work showed good agreement with the results obtained from the linear numerical computer simulators. The results from the two-dimensional numerical computer simulator was also found to be in good agreement with published two-dimensional experimental results.

The numerical simulators were also used to study the effect of some parameters on the steam-drive process. It was found that numerical model results were very sensitive to capillary pressure values. It was also found that the relative permeability data has a minor effect on the results obtained. The oil viscosity was found to affect the process to a large extent. Oil recovery from steam-drive process decreases as the oil viscosity increases. Also, the recovery curves for low viscosity oils show earlier steam breakthrough than those with higher viscosity.

References and illustrations at end of paper.

INTRODUCTION

The first part of the work presented here is a physical laboratory model of steam injection in a linear system. A constant pressure boundary condition was used. Two runs were performed on the same model using two different sets of injection and production pressures. Oil recovery and temperature distribution data were obtained. Each run was repeated to check reproducibility of results.

The second part of this work describes the development and application of numerical simulation techniques to solve equations describing the steam-injection process. This simulation model was the implicit pressure-explicit saturation technique[24,29] to solve difference equations describing the multiphase flow system. The solution of the heat-balance equation yields the temperature ahead of the steam front and the rate of steam condensation behind the front.

THE LINEAR PHYSICAL MODEL

Few linear physical models have been reported in the literature. The most recently published one is that of Willman et al.[23] However, they did not publish enough data so the numerical simulator developed here could be

properly tested. Therefore, a physical model was designed that not only helped in the understanding of the process, but also provided sufficient data to check the simulator.

A schematic diagram of the apparatus is shown in Fig. 1. It consisted of a condensing steam trap, filter, adjustable coil heater, inlet pressure gauge, core holder, thermocouples, outlet pressure gauge, condenser and backpressure regulator.

The steam used in the experiments was a saturated steam from The U. of Texas utility lines. The injection pressure was adjusted by a pressure regulator mounted on the steam lines. The steam coming from the pressure regulator passed through the condensing steam trap. This knocked out the steam condensate. The steam then passed through a filter which removed impurities that could cause clogging of the sand pack. A coil heater was wrapped around the injection line. The temperature of the heater was adjusted by a variable autotransformer to a temperature slightly higher than the saturation temperature of the injected steam. This eliminated any possibility of having condensate in the injected steam.

The oil used was primol 185 with a viscosity of 43 cp at 80°F and at 260°F. Curves of viscosity and specific gravity vs temperature are shown in Fig. 2.

The sand used was an unconsolidated sand of 2.54 darcies permeability and 35.4 percent porosity.

Two steam injection runs were performed using different boundary conditions. The first run was performed with an injection pressure of 40.0 psia and a production pressure of 28.2 psia. The results are plotted in Figs. 3 and 4. The second run was performed with injection pressure of 39.6 psia and production pressure of 14.7 psia. The results are plotted in Figs. 5 and 6. Both runs were repeated and the results were in good agreement.

THE DIFFERENTIAL FORM OF THE PROBLEM

Differential equations describing the fluid and heat flow for the steam-drive process are presented here.

Fluid Flow Equations

The mathematical relationships describing multiphase fluid flow appear in the literature.[5,12,17,20,21] The development of such relationships is based upon mass balance and Darcy's law for each phase. When both relationships are combined, the partial-differential equation describing the fluid flow of each phase in the reservoir will be obtained.

For the oil phase

$$-\frac{\partial(\rho_o u_{xo})}{\partial x}-\frac{\partial(\rho_o u_{yo})}{\partial y}+q_{vo}=\frac{\partial(\phi\rho_o S_o)}{\partial t}\ ; \quad \ldots\ldots\ldots\ldots \text{(1-A)}$$

for the water phase

$$-\frac{\partial(\rho_w u_{xw})}{\partial x}-\frac{\partial(\rho_w u_{yw})}{\partial y}+q_{vw}+q_{vc}=\frac{\partial(\phi\rho_w S_w)}{\partial t}\ ; \quad \ldots\ldots\ldots\ldots \text{(1-B)}$$

and for the steam phase

$$-\frac{\partial(\rho_s u_{xs})}{\partial x}-\frac{\partial(\rho_s u_{ys})}{\partial y}+q_{vs}-q_{vc}=\frac{\partial(\phi\rho_s S_s)}{\partial t}\ , \quad \ldots\ldots\ldots\ldots \text{(1-C)}$$

where u_{xi} and u_{yi} are given by Darcy's law as follows:

$$u_{xi}=-6.33\,\frac{k_x k_{ri}}{\mu_i}\,\frac{\partial p_i}{\partial x} \quad \ldots\ldots \text{(2-A)}$$

$$u_{yi}=-6.33\,\frac{k_y k_{ri}}{\mu_i}\,\frac{\partial p_i}{\partial y} \quad \ldots\ldots \text{(2-B)}$$

and $i = o, w, s$.

Substitution of Eqs. 2 into Eqs. 1 gives

$$6.33\left[\frac{\partial}{\partial x}\left(\frac{k_x k_{ro}\rho_o}{\mu_o}\,\frac{\partial p_o}{\partial x}\right)+\frac{\partial}{\partial y}\left(\frac{k_y k_{ro}\rho_o}{\mu_o}\,\frac{\partial p_o}{\partial y}\right)\right]+q_{vo}=\frac{\partial(\phi\rho_o S_o)}{\partial t} \quad \ldots\ldots\ldots\ldots \text{(3-A)}$$

$$6.33\left[\frac{\partial}{\partial x}\left(\frac{k_x k_{rw}\rho_w}{\mu_w}\,\frac{\partial p_w}{\partial x}\right)+\frac{\partial}{\partial x}\left(\frac{k_y k_{rw}\rho_w}{\mu_w}\,\frac{\rho p_w}{\partial y}\right)\right]+q_{vw}+q_{vc}=\frac{\partial(\phi\rho_w S_w)}{\partial t} \quad \ldots\ldots\ldots\ldots \text{(3-B)}$$

$$6.33\left[\frac{\partial}{\partial x}\left(\frac{k_x k_{rs}\rho_s}{\mu_s}\frac{\partial p_s}{\partial x}\right)+\frac{\partial}{\partial y}\left(\frac{k_y k_{rs}\rho_s}{\mu_s}\frac{\partial p_s}{\partial y}\right)\right]+q_{vs}-q_{vc}=\frac{\partial(\phi\rho_s S_s)}{\partial t} \quad \ldots\ldots\ldots\ldots (3\text{-C})$$

The saturations are related as follows:

$$S_o + S_w + S_s = 1 \quad \ldots\ldots\ldots (4)$$

The pressures of the different phases are related by the capillary pressures as follows:

$$P_{c_{o-w}} = p_o - p_w \quad \ldots\ldots\ldots (5\text{-A})$$

$$P_{c_{o-s}} = p_s - p_o \quad \ldots\ldots\ldots (5\text{-B})$$

All symbols used are described in the Nomenclature.

Heat Flow Equation

The development of the mathematical relationship describing the heat flow in porous media is based upon the heat balance, Fourier, and Darcy's equations. When those equations are combined, the following differential equation is obtained.

$$-\ell_h + \frac{\partial}{\partial x}\left(D_x\frac{\partial Z_n}{\partial x}\right)+\frac{\partial}{\partial y}\left(D_y\frac{\partial Z_n}{\partial y}\right) - \frac{\partial}{\partial x}(u_x\rho h_n) - \frac{\partial}{\partial y}(u_y\rho h_n) + q_{vs}h_{inj} = \frac{\partial}{\partial t}[\phi(\rho Sh) + (1-\phi)\rho_r c_r Z] \quad , (6)$$

where

$$u_i\rho h_n = u_{i_o}\rho_o h_{n_o} + u_{iw}\rho_w h_{n_w} + u_{is}\rho_s h_{n_s} \quad \ldots\ldots\ldots (7)$$

$$S\rho h = S_o\rho_o h_o + S_w\rho_w h_w + S_s\rho_s h_s . \quad (8)$$

and $i = x,y$.

u_{xi} and u_{yi} are given by Eqs 2.

In this study, the functional dependencies of the parameters are assumed to be as follows.

1. Densities of water and oil are functions of temperature only. The density of steam is expressed by the equation

$$\rho_s = \frac{Mp_s}{R(T+460)} \quad , \text{ i.e., an ideal gas.}$$

2. Viscosities of the water, oil and steam depend upon temperature only.

3. Water and steam relative permeabilities are functions of their relative saturations. The oil relative permeability is a function of both oil and water saturations.

4. The capillary pressure between oil and water is a function of the water saturation only. Capillary pressure between oil and steam is a function of both water and oil saturations.

5. The heat loss term is explained in detail in Appendix A. The difference form of the partial-differential equation described here is presented in Appendix B. The application of the IMPES technique to solve the difference equation is given in Appendix C. The equations given in both appendices are for the linear model for simplicity.

DESCRIPTION OF COMPUTER PROGRAMS

The Linear Simulator

The techniques discussed here were incorporated into a Fortran IV computer program. The grid system used is shown in Fig. 7. This program computes at each time step the saturations, pressures and temperature distributions. Also, it computes the steam condensation rates in each block and the injection and production rates. The check for the convergence is based upon the change in pressure, temperature, and steam condensation rates between two successive iterations. Between the three checks, the rate of steam condensation is found to be the controlling one.

The program has a maximum grid-size system of 100. The execution times are dependent on the weight factor used in the calculation of the rate of steam condensation described in Appendix D. A value of 0.85 is found to be most suitable. An average execution time is 0.08 seconds per time step for 10 blocks system on the CDC 6600 computer.

A generalized flow chart of the program is given in Fig. 8. All the necessary data other than the steam viscosity, specific heat, and rock properties are read into the program prior to the main computation loop. At the start of this loop, the relative permeabilities, the capillary pressures, the densities, the viscosities, and the transmissibilities are determined. A table look-up is used for this procedure. In the calculation of the transmissibilities, all the parameters are evaluated 100 percent upstream. Calculation of the pressure distribution then follows. The steam

saturation temperatures are determined from the steam pressures using a table look-up procedure. Calculation of the saturations then follows. Computation of the rate of steam condensation or the temperature is done using the heat balance equation. This is followed by the convergence check.

In the program, steam viscosity, rock density, and specific heats of oil, water and rock are constants. However, steam viscosity and specific heats of oil and water can be used in the program as temperature dependent. Fixing the former quantities is merely due to the relatively small pressure drops used in testing the model.

The Two-Dimensional Simulator

A computer program was written based on the techniques discussed here. The grid system used is shown in Fig. 9. As in the linear simulator, the program computes pressures, saturations and temperature distributions. The program also computes the rate of steam condensation and injection and production rates. Although the controlling parameter in the convergence is the rate of steam condensation, the program computes the change in the three variables, namely, pressure, temperature and rate of steam condensation.

The program has a maximum grid-size system of 20 x 20. Execution times are dependent upon the weight factor used in the calculation of the rate of steam condensation as stated in Appendix D. A value of 0.85 was found to be suitable. An average execution time is 0.25 second per time step on the CDC 6600 computer for a 5 x 5 grid system study.

A generalized flow chart of the program is given in Fig. 8. The program follows the same outline as the linear simulator. However, the values of the parameters in the transmissibilities calculation are taken at the block under consideration except for the relative permeabilities, which are 100 percent upstreamed.

COMPARISON WITH EXPERIMENTAL RESULTS

The Linear Model

As mentioned earlier, two experimental runs with different boundary conditions have been performed. The difference between the runs was the pressure drop. This gave different injection rates, which in turn affected the cumulative heat loss. The pressure level has great significance in the steam-injection process. Saturation temperature and steam enthalpies are functions of pressure level. The higher the pressure level, the higher the temperature level, which, in turn, gives larger rate of heat loss. Data used in the computer program for both experimental runs are given in Appendix F.

The first experiment was performed with a pressure drop of about 11.8 psi and an injection pressure of about 40.0 psia. The experimental and calculated results are plotted in Figs. 3 and 4. The experiment was terminated approximately 40 hours from the start. Although 3 PV had been produced, only about one-half of the model had saturated steam temperature level (Fig. 4). About 84 percent of the oil in place was produced by the end of the experiment.

To test the linear numerical simulator, a computer run was made using the same boundary conditions. Data used in the program are given in Appendix E. The value of the surface over-all thermal coefficient used in the program was aboout double the value determined in the laboratory. However, it was found that the value of the over-all thermal coefficient used behind the steam front is the one that is important in getting a good agreement between the calculated and the experimental results. Accordingly, the difference in values can be due to two factors: (1) the over-all thermal coefficient is temperature dependent to some degree. The value of this coefficient for liquid phases was determined experimentally at 140°F using hot water injection, while the temperature in the steam injection runs reached values up to 270°F and (2) the over-all thermal coefficient for steam is small compared with that for liquids. Steam condensate might have developed a thin layer around the inside wall of the core holder in the region behind the steam front. This will increase the coefficient for this region to some degree.

Results plotted in Fig. 3 show that experimental and calculated results agree closely when the proper value of the over-all thermal coefficient is used.

The second experiment was performed with a pressure drop of 24.9 psi and an injection pressure of 39.6 psia. Both experimental and calculated results are plotted in Figs. 5 and 6. The experiment was terminated after approximately 11 hours. Although only 2 PV were produced, three-fourths of the model had reached steam temperature (Fig. 6). Comparing this result with the one in the former experiment shows the effect of the pressure drop on the heat loss. About 80 percent of oil in place was produced by the end of the experiment.

The linear simulator was run for the boundary conditions of the second experiment. All the parameters used were the same as those used for the first tun, including the value for the surface over-all thermal coefficient.

Results plotted in Fig. 5 show good agreement between experimental and calculated

results when the proper value of the over-all thermal coefficient is used.

The Two-Dimensional Model

The only published results on two-dimensional models are given by Shutler.[20] In his publication, he listed the parameters and the recovery curve for one-eighth of a five-spot model. No temperature distribution was reported. The data are given in Appendix E.

The two-dimensional simulator was used with the data reported. Fig. 10 shows the experimental and the calculated results. A good match between both results is evident.

DISCUSSION

Capillary Pressure

To determine the importance of the capillary pressure in the steam-drive model, two computer runs have been performed using the two-dimensional experiment data given in Appendix E. One run uses the capillary pressures as tabulated in the above mentioned appendix, and the second run uses scaled values, such that

$$P_{c_{scaled}} = \frac{P_{c_{tabulated}}}{10}.$$

The recovery curves are shown in Fig. 10. The recovery curve of the run which uses scaled capillary pressure values shows a delay in the water breakthrough, and an early steam breakthrough when compared with the recovery curve of the run which uses the tabulated values. This might be due to the fact that low capillary pressure values give low steam pressure, which, in turn, give low steam saturation temperature. This will decrease the heat loss that is a function of the temperature levels and accounts for an early steam breakthrough. In this case, more heat will be used to heat the producing zone, giving low oil-to-water viscosity ratio which will result in a delay in the water breakthrough.

The above discussion shows the importance of the capillary pressure values in the steam-drive model. The recovery curve, resulting from the use of scaled capillary pressure values, is closer to the experimental results than the one determined through the use of the tabulated values. To explain such a trend in the results, a comparison was made between the values tabulated and values calculated from Leverett's[9] imbibition J-curve using values of the interfacial tensions at atmospheric conditions. It showed that both are of the same order of magnitude. However, Hough et al.[7] shows that the value of the interfacial tension at the temperature and pressure used in the experiment drops to as low as one-third of its value at atmospheric conditions. This tends to give lower capillary pressure values than the one tabulated.

Relative Permeability

Relative permeability values that are ± 20 percent off the tabulated values in Appendix E have been used in the two-dimensional simulator. The other parameters are the same as those used in the experiment. The recovery curves obtained from both runs show less than 1.2 percent difference. Breakthrough values did not show any change. This indicates that the steam-drive model is not very sensitive to variations on the order of ± 20 percent in relative permeability values.

Oil Viscosity

The steam-drive process has been introduced to the industry as a solution to the problem of producing highly viscous oils; thus, the importance of investigating the effect of viscosity on the process.

Three different oils (I, II, III) with wide ranges of viscosity (Fig. 11) have been used in the two-dimensional simulator. The other parameters are the same as those of the two-dimensional experiment given in Appendix F. The three resulting recovery curves are shown in Fig. 12. The curves show the following.

1. Recovery curves for low viscosity oils show earlier steam breakthrough than those with higher viscosity. This is due to the fact that the driving front moves more slowly in case of high viscosity oils than it moves in case of low viscosity ones. This will increase the heat loss which, in turn, delays the steam breakthrough.

2. Recovery curves for high viscosity oils showed earlier water breakthrough than those with low viscosity. This is due to the fact that for high viscosity oils, the mobility of water is much greater than the mobility of oil, which will accelerate the water production.

3. Although oil recovery from steam-drive process decreases as the oil viscosity increases, it still gives much higher values than those obtained from the waterflood process. The recovery curve for a waterflood in a five-spot pattern and for oil-to-water viscosity ratio of 754 is shown in Fig. 10. Such oil is comparable to the one used in the two-dimensional experiment. Comparing the two recovery curves shows the superiority of the steamflood process over the waterflood process. However, as mentioned before, the recovery curves of the steamflood process differ considerably with the magnitude of the heat loss.

NOMENCLATURE

A = cross-sectional area, sq ft
c = specific heat, Btu/lb day °F
f = fractional flow, dimensionless
H = reservoir sand thickness, ft
h = enthalpy, Btu/lb
h_{inj} = enthalpy of injected steam, Btu/lb
k = absolute permeability, darcies
k_r = relative permeability, dimensionless
$\mathcal{L}_h$ = heat loss, Btu/D
M = molecular weight of steam
p = pressure, psia
P_c = capillary pressure, psi
q = mass injection rate, lb/D
q_v = volumetric injection term, lb/unit bulk reservoir volume per day
R = gas constant, psia/cu ft lb mol °R
r = radius
R = heat residual, Btu/D
S = saturation, dimensionless
T = temperature, °F if not subscripted, and transmissibility if subscripted, lb/D psi
t = time, days
u = Darcy's velocity, ft/D
U = over-all thermal coefficient, Btu/D Sq ft °F
v_p = block pore volume, cu ft
x,y,z = Cartesian coordinates, ft

Greek

Δ = difference operator
μ = viscosity, cp
η = dimensionless height
ϕ = porosity, dimensionless
ρ = density, lb/cu ft
τ = dimensionless time

Subscripts

a = ambient condition
c = condensate
i = grid index in the x-direction
j = grid index in the y-direction
$\mathcal{L}$ = liquid
n = old-time step
n+1 = new-time step

REFERENCES

1. Buckley, S. E. and Leverett, M. C.: "Mechanism of Fluid Displacement in Sands", Trans., AIME (1942) 146, 107-116.
2. Coats, K. H.: "Computer Simulation of Three-Dimensional Three-Phase Flow in Reservoirs", Unpublished Report, The U. of Texas at Austin (Nov., 1968).
3. Coats, K. H.: P. En. 383.21 class notes, Petroleum Engineering Dept., The U. of Texas at Austin (1967).
4. Coats, K. H.: Private Communication (1968).
5. Coats, K. H., Nielsen, R. L., Terhune, M. H. and Weber, A. G.: "Simulation of Three-Dimensional, Two-Phase Flow in Oil and Gas Reservoirs", Soc. Pet. Eng. J. (Dec., 1967) 377-388.
6. Higgins, R. V. and Leighton, A. J.: "A Computer Method to Calculate Two-Phase Flow in Any Irregularly Bounded Porous Medium", J. Pet. Tech. (June, 1962) 679-683.
7. Hough, E. W., Rzasa, M. J. and Wood, B. B.: "Interfacial Tensions at Reservoir Pressures and Temperatures, Apparatus and the the Water-Methane System", Trans., AIME (1951) 192, 57-60.
8. Lauwerier, H. A.: "The Transport of Heat in an Oil Layer Caused by the Injection of Hot Fluid", Applied Sci. Res. (1955) Sec. A, 5, 145.
9. Leverett, M. C.: "Capillary Behavior in Porous Solids", Trans., AIME (1941) 142, 152-169.
10. Little, T. W.: "Recovery of Viscous Crude Oil by In Situ Combustion", MS thesis, Petroleum Engineering Dept., The U. of Texas (July, 1958).
11. Marx, J. W. and Langenheim, R. H.: "Reservoir Heating by Hot Fluid Injection", Trans., AIME (1959) 216, 312-315.
12. MacDonald, R. C. and Coats, K. H.: "Methods for Numerical Simulation of Water and Gas Coning", Soc. Pet. Eng. J. (Dec., 1970) 425-436.
13. Ramey, H. J.: Discussion on "Reservoir Heating by Hot Fluid Injection", Trans., AIME (1959) 216, 364-365.
14. Ramsey, P. E.: "Recovery of Viscous Crude Oil by Steam Injection", MS thesis, Petroleum Engineering Dept., The U. of Texas (May, 1958).
15. Reid, S.: "The Flow of Three Immiscible Fluids in Porous Media", PhD dissertation, Chemical Engineering Dept., U. of Birmingham (1956).
16. Richtmyer, R. D.: Difference Methods for Initial-Value Problems, Interscience Publishers, New York (1957) 101.
17. Sheldon, J. W., Harris, C. D. and Bavly, D.: "A Method for General Reservoir Behavior Simulation on Digital Computers", Paper SPE 1521-G presented at the 35th Annual SPE Fall Meeting, Denver, Oct. 2-5, 1960.
18. Snell, R. W.: "Three-Phase Relative Permeability in an Unconsolidated Sand", J. Inst. Pet. (March, 1962) 48, 80.
19. Shutler, N. D.: "Numerical, Three-Phase Simulation of the Linear Steamflood Process", Soc. Pet. Eng. J. (June, 1969) 232-246.
20. Shutler, N. D.: "Numerical Three-Phase Model of the Two-Dimensional Steam Flood Process", Soc. Pet. Eng. J. (Dec., 1970) 405-417.
21. Spillette, A. G. and Nielsen, R. L.: "Two-Dimensional Method for Predicting Hot Waterflood Recovery Behavior", J. Pet. Tech.

(June, 1968) 627-638.
22. Stone, H. L. and Garder, A. D., Jr.: "Analysis of Gas-Cap or Dissolved-Gas Drive Reservoirs", Soc. Pet. Eng. J. (June, 1961) 92-104.
23. Willman, B. T., et al.: "Laboratory Studies of Oil Recovery by Steam Injection", J. Pet. Tech. (July, 1961) 681-690.

APPENDIX A

Heat Loss Calculation

In the computer simulator developed in this study two procedures are used to calculate the heat loss. One is used in the testing of the physical models, and the other is used in the field case studies.

Heat Loss Calculation for the Physical Models

Physical models are made with limited insulation thickness. A representation of the heat loss in terms of an average over-all thermal coefficient that can be determined in the laboratory will best suit such cases. The following is the equation used for cylindrical insulations around a cylindrical core holder:

$$\text{Heat loss} = \pi\, d\, U\, Z\, x, \quad \ldots\ldots (A\text{-}1)$$

where d = outside diameter of the insulation, ft
U = over-all thermal coefficient, Btu/D sq ft ^{o}F
Z = difference in temperature across the insulation, ^{o}F
x = block length, ft

Since the over-all thermal coefficient of steam is different than that of liquids, a weighted average value was used in this study and is given by the following equation:

$$U_{av} = U_s S_s + U_l (1 - S_s) \quad \ldots\ldots (A\text{-}2)$$

Heat Loss Calculation for Field Cases

In field cases, the overburden and the underburden can be considered as infinite insulations. The equations under consideration are those describing the heat flow in a semi-infinite slab. Their solution is made using Laplace transforms

Consider a reservoir sand of thickness h. The z-axis runs parallel to the heat flowing to the overburden as in the figure. The partial-differential equation describing the heat flow is as follows:

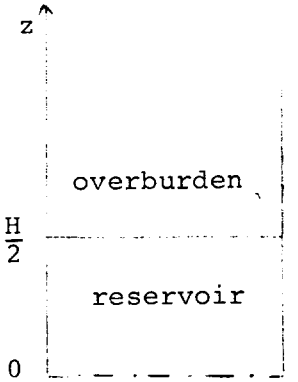

$$K_z \frac{\partial^2 T}{\partial z^2} = \rho_r c_r \frac{\partial T}{\partial t} \quad \ldots\ldots\ldots (A\text{-}3)$$

The boundary conditions are

$$T = T_i \text{ at } z = \frac{H}{2} \text{ and } t = t_i \quad \ldots (A\text{-}4)$$

$$T \to T_a \text{ as } z \to \infty \quad \ldots\ldots\ldots (A\text{-}5)$$

The initial condition is

$$T = T_a \text{ at } t = 0 \text{ and all } z \quad \ldots (A\text{-}6)$$

Let

$$\tau = \frac{4 K_z t}{H^2 \rho_r c_r} \quad \ldots\ldots\ldots\ldots (A\text{-}7)$$

$$\eta = \frac{z}{H/2} \quad \ldots\ldots\ldots\ldots (A\text{-}8)$$

$$Z = T - T_a \quad \ldots\ldots\ldots\ldots (A\text{-}9)$$

Then Eqs. A-3 through A-6 will be

$$\frac{\partial^2 Z}{\partial \eta^2} = \frac{\partial Z}{\partial \tau} \quad \ldots\ldots\ldots\ldots (A\text{-}10)$$

$$Z = Z_i \text{ at } \eta = 1 \text{ and } \tau = \tau_i \quad \ldots (A\text{-}11)$$

$$Z \to 0 \text{ as } \eta \to \infty \quad \ldots\ldots\ldots (A\text{-}12)$$

$$Z = 0 \text{ at } \tau = 0 \text{ and all } \eta \quad \ldots (A\text{-}13)$$

Performing Laplace transform on Eqs. A-10 and A-11 and using Eq. A-13 we get

$$\frac{\partial \bar{Z}}{\partial \eta^2} - S\bar{Z} = 0 \quad \ldots\ldots\ldots\ldots (A\text{-}14)$$

$$\bar{Z} = \frac{Z_i}{S} \text{ at } \eta = 1 \text{ and } \tau = \tau_i \quad \ldots (A\text{-}15)$$

The solution to Eq. A-14 is

$$\bar{Z} = c_1 e^{\eta\sqrt{s}} + c_2 e^{-\eta\sqrt{s}} \quad \ldots\ldots (A\text{-}16)$$

Eq. A-12 gives $c_1 = o$. Then equation A-16 will be

$$\bar{Z} = c_2 e^{-\eta\sqrt{s}} \quad \ldots\ldots\ldots\ldots (A\text{-}17)$$

Using Eq. A-15 in Eq. A-17, we get

$$\frac{Z_i}{S} = c_2 e^{-\sqrt{s}}$$

then

$$c_2 = \frac{Z_i}{S} e^{\sqrt{s}}$$

and

$$\bar{Z} = Z_i \frac{e^{-(\eta-1)\sqrt{s}}}{s} \quad \ldots\ldots\ldots (A\text{-}18)$$

Performing the inverted Laplace transform to Eq. A-18, we get

$$Z(\eta,\tau) = Z_i \operatorname{erfc} \frac{\eta-1}{2\sqrt{\tau}} \quad \ldots\ldots (A\text{-}19)$$

Using Leipnitz rule to differentiate Eq. A-19, we get

$$\frac{\partial Z}{\partial \tau} = \frac{Z_i(\eta-1)}{2\sqrt{\pi}} \frac{e^{\frac{-(\eta-1)^2}{4\tau}}}{\sqrt{\pi^3}} \quad \ldots\ldots (A\text{-}20)$$

$$\text{Rate of heat loss per unit volume} = \rho_r c_r \int_1^\infty \frac{\partial Z}{\partial t}$$

$$= \frac{2K_z Z_i}{h^2 \tau\sqrt{\pi\tau}} \int_1^\infty (\eta-1)\, e^{\frac{-(\eta-1)^2}{4\tau}} = \frac{4K_z Z_i}{h^2\sqrt{\pi\tau}} \cdot \quad \ldots\ldots\ldots\ldots (A\text{-}21)$$

Eq. A-21 gives the rate of heat loss per unit volume.

APPENDIX B

Finite-Difference Expansion

Before starting any finite-difference expansion, the grid system must be specified. The selection of such a system depends upon the boundary conditions to be used.

For the linear model to be developed here, predetermined injection and production pressures will be used as boundary conditions. The grid system shown in Fig. 7 is the most suitable for this case. All finite-difference expansions that follow in this chapter pertain to such a grid system.

Eqs. 3 contain second-order spatial derivatives and first-order time derivatives. The standard central-difference approximation for the spatial derivatives is as follows.

$$\frac{\partial}{\partial x}\left(a_O \frac{\partial p_O}{\partial x}\right) \cong \frac{a_{O_{i+1/2}}\left(p_{O_{i+1}} - p_{O_i}\right) - a_{O_{i-1/2}}\left(p_{O_i} - p_{O_{i-1}}\right)}{\Delta x^2} \quad \ldots\ldots\ldots\ldots (B\text{-}1)$$

where

$$a_O = \frac{k_x k_{rO} \rho_O}{\mu_O} \quad \ldots\ldots\ldots\ldots (B\text{-}2)$$

The p_O values in these spatial differences are understood to apply at the new time level t_{n+1}.

The backward time difference approximation is used for the time derivatives as follows:

$$\frac{\partial}{\partial t}(\phi \rho_O S_O) \cong \frac{(\phi \rho_O S_O)_{n+1} - (\phi \rho_O S_O)_n}{\Delta t}. \quad \ldots\ldots\ldots\ldots\ldots\ldots (B\text{-}3)$$

Using these finite-difference approximations in Eq. 3 and multiplying both sides of the equation by $A\Delta x$, we get

$$\Delta_x T_O \Delta_x p_O = \frac{v_p}{\Delta t}\Delta_t(\rho_O S_O) \quad . (B\text{-}4a)$$

$$\Delta_x T_w \Delta_x p_w + q_c = \frac{v_p}{\Delta t}\Delta_t(\rho_w S_w) \quad . (B\text{-}4b)$$

$$\Delta_x T_s \Delta_x p_s - q_c = \frac{v_p}{\Delta t}\Delta_t(\rho_s S_s) \quad . (B\text{-}4c)$$

where

$$\Delta_x T_O \Delta_x p_O = T_{O_{i+1/2}}\left(p_{O_{i+1}} - p_{O_i}\right) - T_{O_{i-1/2}}\left(p_{O_i} - p_{O_{i-1}}\right) \quad \ldots\ldots\ldots\ldots\ldots (B\text{-}5)$$

$$T_{O_{i+1/2}} = 6.33 \frac{A}{\Delta x} \frac{k_x k_{rO} \rho_O}{\mu_O}_{i+1/2} \quad (B\text{-}6)$$

and A is the cross-sectional area perpendicular to the flow.

Applying the same finite-difference approximations to the heat-balance Eq. 6 and multiplying both sides by $A\Delta x$, we get

$$\frac{D_x A}{\Delta x}\Delta_x^2 Z_n - l_n - A\Delta_x(u\rho h_n) + q_s h_{inj} = \frac{v_p}{\Delta t}\Delta_t\left(s\rho h + \frac{1-\phi}{\phi}\rho_r c_r z\right), \quad . (B\text{-}7)$$

where

$$\Delta_x(u_O \rho_O h_O) = A(u_O\rho_O)_{i+1/2} h_{no_i} - A(u_O\rho_O)_{i-1/2} h_{no_{i-1}} \quad \ldots\ldots\ldots\ldots\ldots\ldots (B\text{-}8)$$

$$A(u_O\rho_O)_{i+1/2} = T_{O_{i+1/2}}\left(p_{O_{i+1}} - p_{O_i}\right) \quad \ldots\ldots\ldots\ldots\ldots\ldots (B\text{-}9)$$

$$\Delta_t(\rho_O S_O h_O) = (\rho_O S_O h_O)_{n+1} - (\rho_O S_O h_O)_n \quad \ldots\ldots\ldots\ldots\ldots\ldots \text{(B-10)}$$

$$\Delta_x^2 Z_n = Z_{n_{i+1}} - 2\,Z_{n_i} + Z_{n_{i-1}}. \quad \text{(B-11)}$$

APPENDIX C

IMPES Application

IMPES is a technique in which the pressure in the flow term, $\Delta T \Delta p$, is handled implicitly, while the saturation and saturation-dependent parameters are handled explicitly. This technique is described in the literature.[17,22] In this analysis this technique is applied in a manner described by Coats.[2]

Eq. B-4 can be rewritten as follows.

$$\Delta_x T_O \Delta_x p_O =$$

$$\frac{v_p}{\Delta t}\rho_{O_{n+1}}\Delta_t S_O + \frac{v_p}{\Delta t} S_{O_n}\Delta_t \rho_O \quad \text{(C-1a)}$$

$$\Delta_x T_w \Delta_x p_w + q_c =$$

$$\frac{v_p}{\Delta t}\rho_{w_{n+1}}\Delta_t S_w + \frac{v_p}{\Delta t} S_{w_n}\Delta_t \rho_w \quad \text{(C-1b)}$$

$$\Delta_x T_s \Delta_x p_s - q_c =$$

$$\frac{v_p}{\Delta t}\rho_{s_{n+1}}\Delta_t S_s + \frac{v_p}{\Delta t} S_{s_n}\Delta_t p_s \quad \text{(C-1c)}$$

Multiplying Eq. C-1b by a_1 and Eq. C-1c by a_3 and adding the three equations, we get

$$\Delta_x T_O \Delta_x p_O + a_1 \Delta_x T_w \Delta_x p_w + a_3 \Delta_x T_s \Delta_x p_s + (a_1 - a_3) q_c = \frac{v_p}{\Delta t}\Big[\rho_{O_{n+1}}\Delta_t S_O + a_1\rho_{w_{n+1}}\Delta_t S_w + a_3\rho_{s_{n+1}}\Delta_t S_s = \frac{v_p}{\Delta t}\Big[S_{O_n}\Delta_t\rho_O + a_1 S_{w_n}\Delta_t\rho_w + a_3 S_{s_n}\Delta_t\rho_s \quad \ldots\ldots\ldots \text{(C-2)}$$

Using Eq. 4 and choosing a_1 and a_3 such that

$$\left(a_1\rho_{w_{n+1}} - a_3\rho_{s_{n+1}}\right)\Delta_t S_w + \left(\rho_{O_{n+1}} - a_3\rho_{s_{n+1}}\right)\Delta_t S_O = 0 \ ,$$

then

$$a_3 = \frac{\rho_{O_{n+1}}}{\rho_{s_{n+1}}} \quad \ldots\ldots\ldots\ldots \text{(C-3a)}$$

$$a_1 = a_3\frac{\rho_{s_{n+1}}}{\rho_{w_{n+1}}} \quad \ldots\ldots\ldots\ldots \text{(C-3b)}$$

Substituting Eq. 5 in Eq. 13, we get

$$\Delta_x T \Delta_x p_O - a_1\Delta_x T_w \Delta_x P_{c_{O-w}} + a_3\Delta_x T_s \Delta_x P_{c_{s-O}} + (a_1 - a_3)q_c = \frac{v_p}{\Delta t}(a_1 S_{w_n}\Delta_t\rho_w + S_{O_n}\Delta_t\rho_O + a_3 S_{s_n}\Delta_t\rho_s), \quad \ldots\ldots\ldots \text{(C-4)}$$

where

$$T = a_1 T_w + T_O + a_3 T_s \quad \ldots\ldots \text{(C-5)}$$

In forming $\Delta_x T \Delta_x p_O$, care must be taken in leaving a_1 and a_3 outside the spatial difference.

Since oil and water densities have been considered in this study to be functions of temperature only and steam density is a function of both temperature and pressure, the term $\Delta_t\rho_s$ can further be expanded as follows:

$$\Delta_t\rho_s = \Delta_t\rho_s^* + \rho_s'\Delta_t p \ , \quad \ldots\ldots \text{(C-6)}$$

where

$$\Delta_t\rho_s^* = \rho_s(Z_{n+1}, p_{s_n}) - \rho_s(Z_n, p_{s_n}) \quad \text{(C-7)}$$

$$\rho_s' = \frac{\rho_s(Z_{n+1}, p_{n+1}) - \rho_s(Z_{n+1}, p_{s_n})}{p_{s_{n+1}} - p_{s_n}} \quad \ldots\ldots\ldots\ldots\ldots\ldots \text{(C-8)}$$

From Eqs. C-4 and C-6 we get the following:

$$\Delta_x T \Delta_x p_O^{k+1} + B^k = G\Delta_t p_O \ , \quad \ldots \text{(C-9)}$$

where

$$B^k = (a_1 - a_3)q_c^k - a_1\Delta_x T_w \Delta_x P_{c_{O-w}} + a_3\Delta_x T_s \Delta_x P_{c_{s-O}} - \frac{v_p}{\Delta t}[a_1 S_{w_n}\Delta_t\rho_w$$

$$+ S_{o_n} \Delta_t \rho_o + a_3 S_{s_n} \Delta_t \rho_s^*] \quad . . \quad (C\text{-}10)$$

and

$$G = \frac{v_p}{\Delta t} a_3 S_{s_n} \rho_s' \quad . \quad . \quad . \quad . \quad . \quad . \quad . \quad . \quad (C\text{-}11)$$

The superscript (k) shows that the value at the old iteration is to be used. The superscript (k+1) shows that the value at the new iteration is to be used.

APPENDIX D

Rate of Steam Condensation

The calculation of the rate of steam condensation is made by the use of two sets of equations. The first set is for blocks that have no free steam, i.e., their temperatures are below the saturation temperatures of steam. The second set of equations is for blocks that have free steam, i.e., their temperatures are equal to the saturation temperatures of steam.

Blocks with No Free Steam

In these blocks, all the steam coming in from adjacent blocks is condensing, i.e.,

$$q_c = T_{s_{x_{i-1/2,j}}} \cdot (p_{s_{i-1,j}} - p_{s_{i,j}}) + T_{s_{y_{i,j-1/2}}} (p_{s_{i,j-1}} - p_{s_{i,j}}) \quad . \quad . \quad . \quad . \quad . \quad . \quad . \quad . \quad . \quad . \quad . \quad . \quad . \quad . \quad . \quad . \quad . \quad . \quad . \quad (D\text{-}1)$$

Blocks with Free Steam

After solving the fluid flow equations for the pressure distribution, the steam saturation temperatures for blocks with free steam are determined. The use of these temperatures in the heat-balance equation will result in residuals. These residuals are due to the use of the rate of steam condensation at the old iteration in solving the fluid flow equations. Correction of such values will reduce the residuals to within limits of tolerance.

Denoting the residual of the heat-balance equation at any grid point by R, we then have

$$q_c^{k+1} = q_c^k + \frac{R}{h_s - h_w} \cdot wf \ ,$$

where (wf) is a weight factor to be chosen in a way that will accelerate the convergence.

APPENDIX E

Data Used for Calculations

This appendix contains data used in the operational models. The relative permeabilities, capillary pressures and dispersion coefficients for the linear model study are obtained from Shutler.[20]

E.1 Linear Experiment I

E.2 Linear Experiment II

E.3 Two-dimensional experiment

	E.1	E.2	E.3
k (darcys)	2.54	2.54	132
	.354		.372
L (ft.)	3.42		3.9
H (ft.)			.83
U_L (Btu/day.ft. F)	6.2	6.2	
U_s (Btu/day.ft. F)	.204	.204	
D (Btu/ft.day. F)	80	80	24
P_r (Number/ft.^{3})	167	167	167
C_r (Btu/lb. F)	.1855	.1855	.2156
T_a (F)	80	80	80
S_{w_i}	.229	.229	.1

	E.1	E.2	E.3
T_{inj} (F)	267.25	266.63	400
P_{inj} (Psi)	25.3	24.9	260
P_{prod} (Psi)	13.5	0	190

E.1 and E.2

S_w	$P_{c_{o-w}}$	$\bar{S}_o$	$P_{c_{s-o}}$
.2287	2.2	.3	.38
.30	1.0	.4	.29
.40	.7	.5	.21
.50	.52	.6	.16
.60	.37	.7	.12
.70	.23	.8	.11
.90	.1		

S_w	k_{rw}	$k_{ro_{o-w}}$
.2287	0	1.0
.3	.002	.922
.4	.009	.8
.5	.012	.58
.6	.019	.26
.7	.022	.06
.9	.042	0.0

$\bar{S}_o$	$k_{ro_{s-o}}$	k_{rs}
.2	.0008	.175
.4	.01	.105
.5	.04	.05
.6	.125	.01
.7	.38	.001
.8	.7	.0

E.3

S_w	$P_{c_{o-w}}$	$\bar{S}_o$	$P_{c_{s-o}}$
.1	4.1	.1	4.517
.2	.095	.2	.067
.3	.072	.3	.042
.4	.061	.4	.02
.5	.051	.5	-.001
.6	.041	.6	-.022
.7	.031	.7	-.043
.8	.021	.8	-.064
.86	.011	.89	-.085

S_w	k_{rw}	$k_{ro_{o-w}}$
.1	0	1.0
.2	.0016	.875
.3	.0081	.735
.4	.0259	.590
.5	.0672	.42
.6	.1	.21
.7	.14	.07
.8	.20	.016
.86	.25	0

$\bar{S}_o$	$k_{ro_{s-o}}$	k_{rs}
.1	0	.52
.2	.009	.41
.3	.031	.31
.4	.062	.22
.5	.11	.14
.6	.19	.08
.7	.335	.03
.8	.570	.005
.89	1.0	0

Temperature	Viscosity (Cp)
80	800
100	330
140	110
180	46
240	18
280	11
360	5.26
450	2.9

TABLE 1 - RESULTS OF EXPERIMENT 1, LINEAR MODEL, PORE VOLUME = 494.14cc

Time (min.)	Pressure (Psi)		Fluids Produced (cc)		Temperature F					
					Distance from Inlet					
	Inlet	Outlet	Oil	Total	1.2"	8.9"	16.6"	23.3"	31"	38.7"
0	25.2	13.4	0	0	80	80	80	80	80	80
30	25.1	13.3	6.6	6.6	84	80	80	80	80	80
60	25	13.2	13.4	13.4	96	80	80	80	80	80
90	25.1	13.2	20.3	20.3	107	80	80	80	80	80
120	25.2	12.9	27.9	27.9	116	80	80	80	80	80
150	25.2	13.2	35.8	35.8	124	80	80	80	80	80
180	25.1	13.3	42.9	42.9	132	84	80	80	80	80
210	25.2	13.1	50	50	137	85	80	80	80	80
240	25.3	13.2	57.8	57.8	138	88	80	80	80	80
270	25.3	12.8	68.2	68.2	142	90	80	80	80	80
300	25.3	12.9	77.5	77.5	147	92	80	80	80	80
330	25.2	12.8	87.6	87.6	154	93	80	80	80	80
360	25.2	13.2	98.5	98.5	161	96	80	80	80	80
390	25.2	13	109.2	109.2	168	98	80	80	80	80
420	25.2	13.2	121	121	174	100	81	80	80	80
450	25.2	13.1	134.8	134.8	183	101	82	80	80	80
480	25.2	13.1	149.8	149.8	192	105	83	80	80	80
510	24.8	13.1	171	171	200	108	85	81	80	80
540	24.9	13.3	191.8	191.8	205	112	86	80	80	80
570	24.9	13.1	205	219.5	258	117	87	80	80	80
600	24.9	13.1	212	260.5	279	125	88	80	80	80
640	24.9	13.2	221.3	309.3	279	144	90	82	80	80
680	24.9	13.2	226.5	358.5	279	180	98	83	80	80
720	24.8	13.2	232.5	408	279	223	106	84	80	80
760	24.8	13.2	237	454	279	247	115	86	80	80
800	24.9	13.2	241.5	503	279	275	128	90	80	80
850	24.9	13.1	247.6	564	279	275	143	95	82	80
880	24.9	13.2	250.9	599.2	279	275	152	99	82	80
910	24.9	13.2	254.9	636.7	279	275	162	102	83	80
940	24.4	13.0	259.1	676.6	279	275	172	106	84	80
970	24.9	13.2	263.6	715.5	279	275	182	109	86	80
1000	24.9	12.9	268.4	753.9	279	275	192	117	89	80
1030	24.8	12.8	272.5	790.6	279	275	199	119	90	80
1060	24.4	13.3	277.3	830.6	279	275	211	124	92	80
1090	24.8	13	282.3	874.8	279	275	228	129	94	83
1120	24.9	13	287.4	917.4	279	275	244	135	98	84
1180	24.8	12.8	295.8	1008.1	279	275	266	149	102	85
1210	24.8	12.9	298.3	1050.6	279	275	266	157	104	85
1240	24.8	12.9	301.8	1095.4	279	275	266	164	106	86
1270	24.8	12.8	305.3	1140.1	279	275	266	170	108	86
1305	24.8	12.8	308.9	1186.7	279	275	266	175	110	86
1345	24.8	12.3	312.9	1251.7	279	275	266	184	114	86
1385	24.8	12.2	317.4	1310.2	279	275	266	198	123	92
1430	24.8	13.0	321	1360.5	279	275	266	205	127	93
1460	24.9	13.0	324	1406.4	279	275	266	210	130	94
1500	24.8	13.0	326.2	1451.6	279	275	266	212	134	98

TABLE 2 - RESULTS OF EXPERIMENT 2, LINEAR MODEL, PORE VOLUME = 494.14cc

Time (min.)	Pressure (Psi)		Fluids Produced (cc)		Temperature F					
					Distance from Inlet					
	In-let	Out-let	Oil	Total	1.2"	8.9"	16.6"	23.3"	31"	38.7"
0	24.8	0	0	0	80	80	80	80	80	80
40	25.3	0	20.4	20.4	110	80	80	80	80	80
80	24.8	0	41.2	41.2	133	83	80	80	80	80
120	24.7	0	65	65	151	88	80	80	80	80
160	24.7	0	91.5	91.5	176	96	80	80	80	80
200	24.5	0	122.7	122.7	210	104	84	80	80	80
240	24.3	0	160.3	160.3	279	116	88	80	80	80
280	24.6	0	183.2	222	279	170	92	84	80	80
320	24.8	0	207.5	305.5	279	254	102	86	80	80
360	24.8	0	222.1	381.8	279	275	172	90	80	80
400	24.9	0	237.3	448	279	275	264	106	84	80
440	24.9	0	247.2	514.6	279	275	265	144	90	80
480	24.8	0	262.6	594.8	279	275	265	170	98	80
520	24.9	0	275.5	677.7	279	275	265	254	120	80
560	24.8	0	286.4	768.2	279	275	265	254	166	96
600	24.9	0	297.3	849.6	279	275	265	254	214	102
640	24.9	0	306.1	929.1	279	275	265	254	236	124

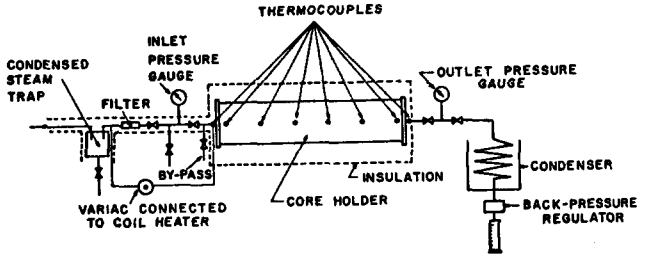

Fig. 1 - Schematic diagram of the apparatus.

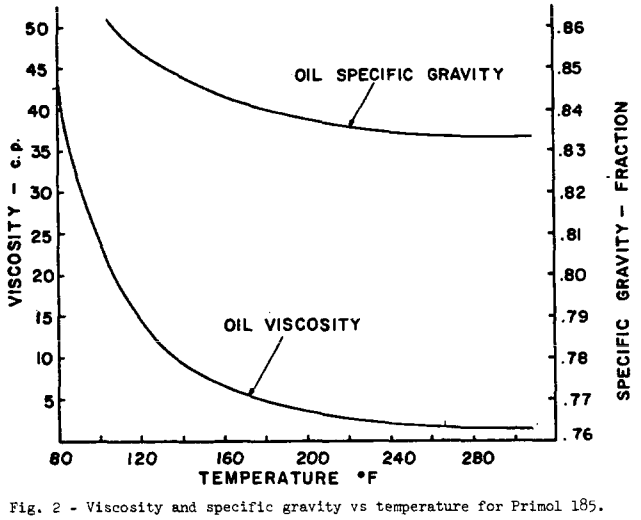

Fig. 2 - Viscosity and specific gravity vs temperature for Primol 185.

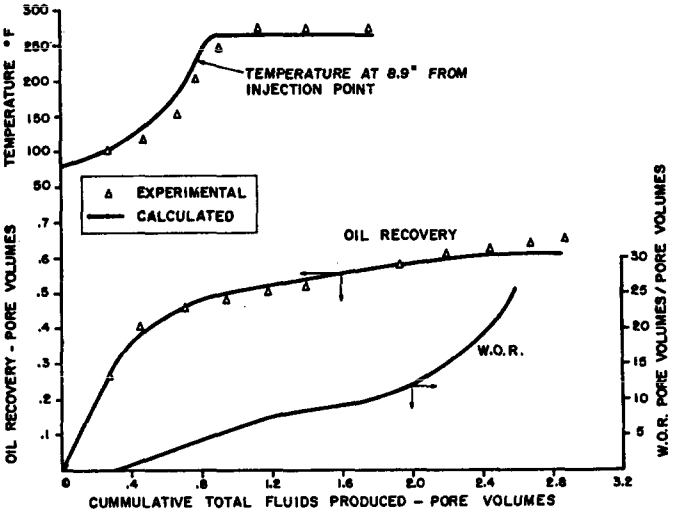

Fig. 3 - Experimental and calculated results of linear Experiment 1, Δp = 11.8 psi.

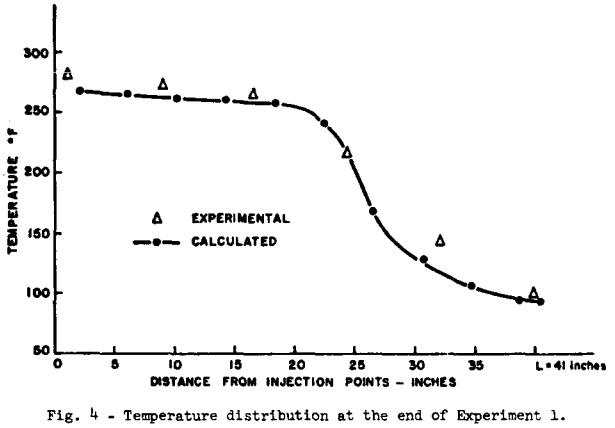

Fig. 4 - Temperature distribution at the end of Experiment 1.

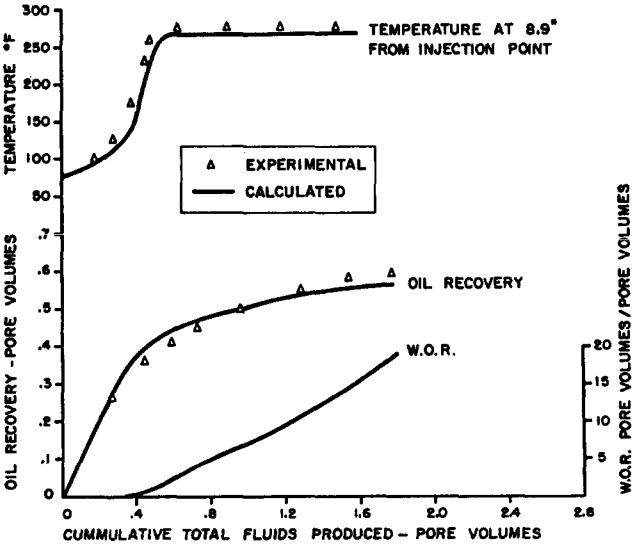

Fig. 5 - Experimental and calculated results of linear Experiment 2, Δp = 24.9 psi.

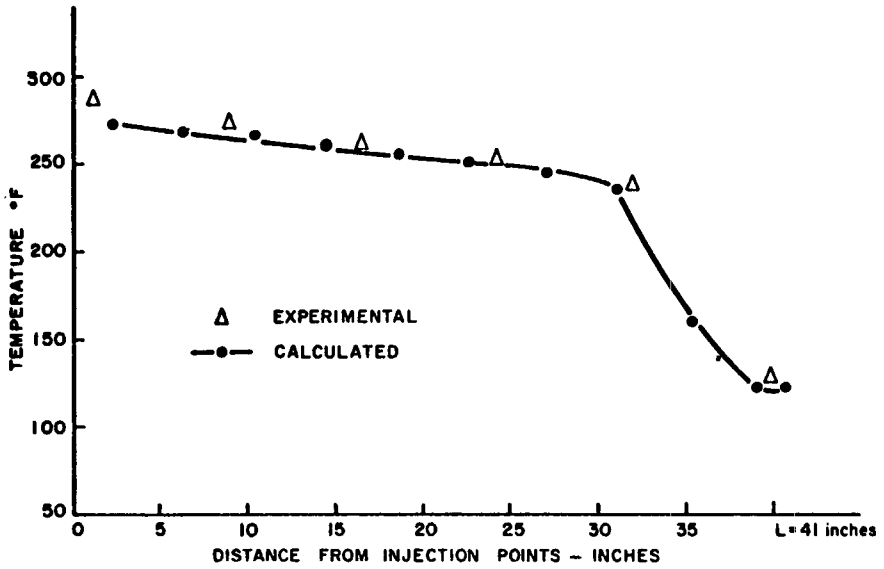

Fig. 6 - Temperature distribution at the end of Experiment 2.

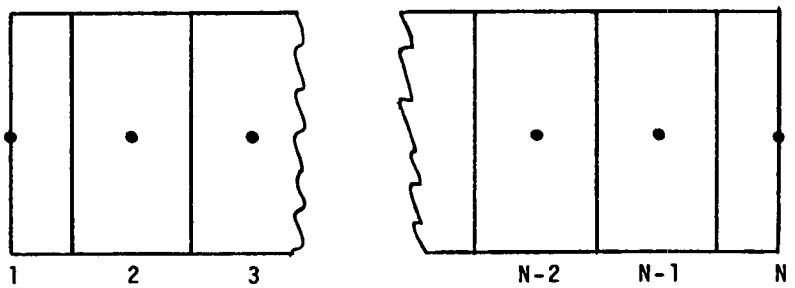

Fig. 7 - Grid system used in the linear numerical simulator.

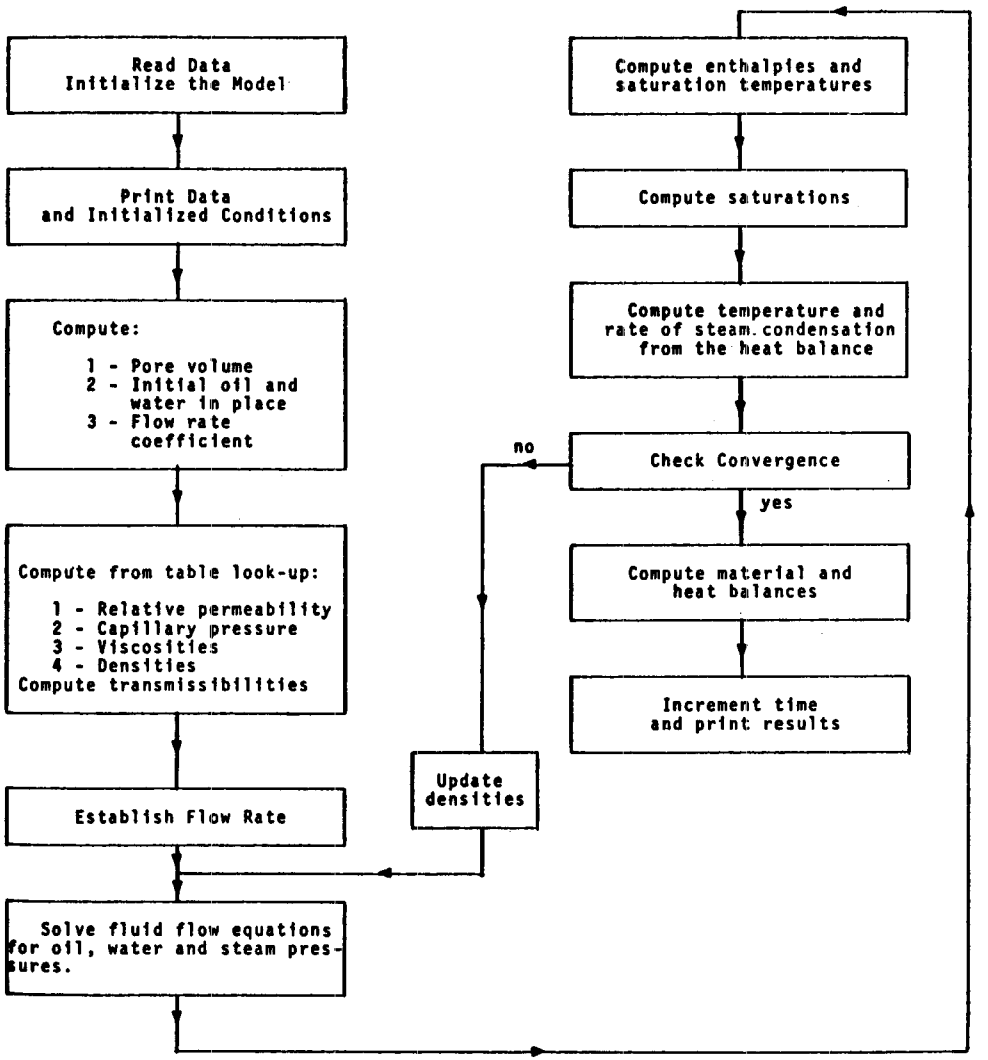

Fig. 8 - Numerical simulators flow chart.

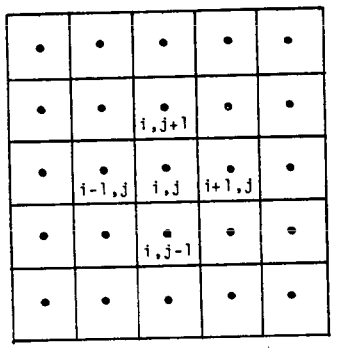

Fig. 9 - Grid system used in the two-dimensional numerical simulator.

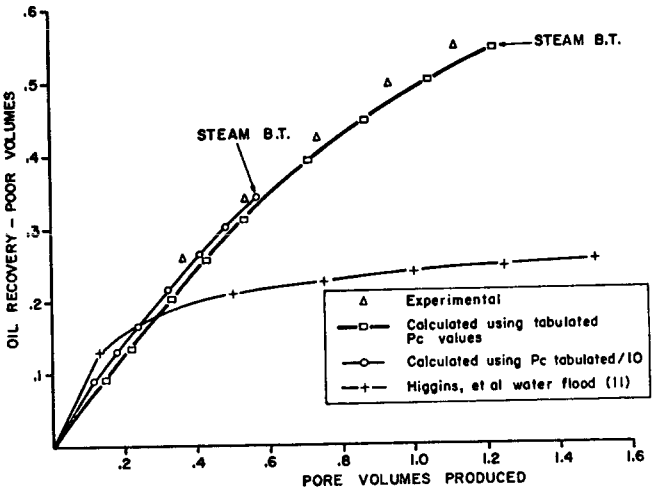

Fig. 10 - Experimental and calculated results of the two-dimensional experiment.

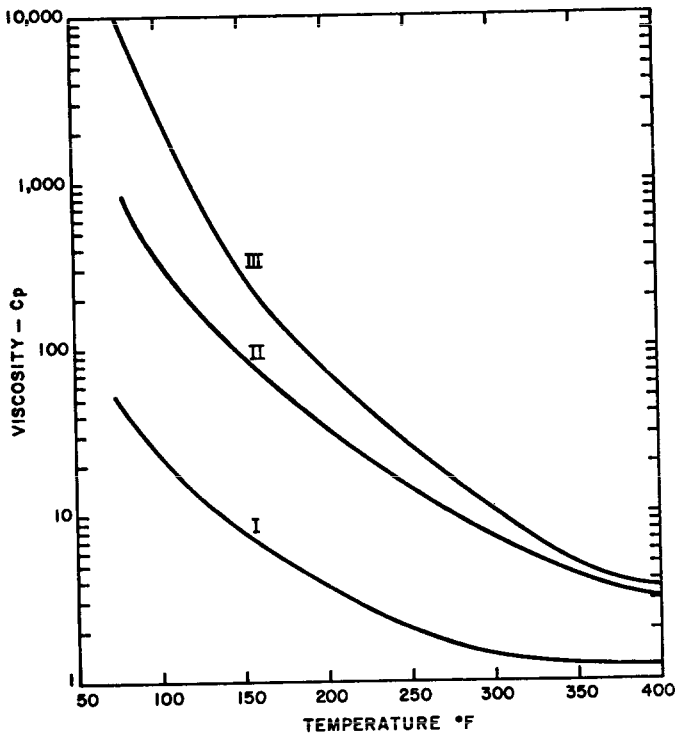

Fig. 11 - Viscosity vs temperature.

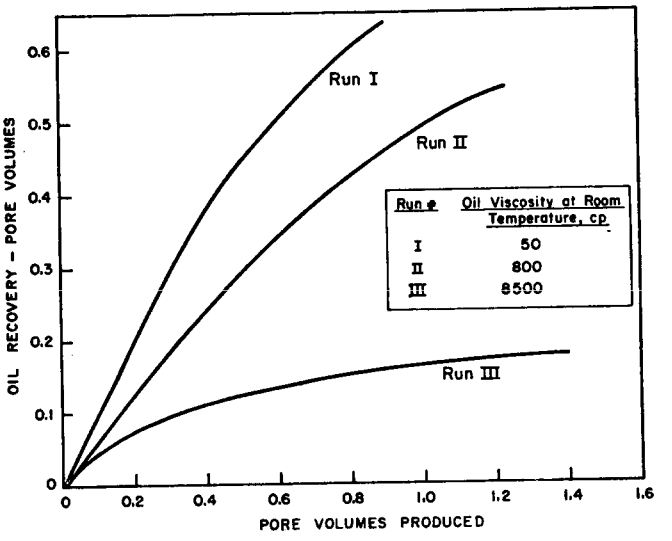

Fig. 12 - Computed oil recovery curves for different oil viscosities.